Bidomain ECG Simulations Using an Augmented Monodomain Model for the Cardiac Source

Martin J. Bishop and Gernot Plank*

***Abstract*—The electrocardiogram (ECG) is an essential clinical tool for the noninvasive assessment of cardiac function. Computational simulations of ECGs using bidomain models are considered the biophysically most detailed approach, but computational costs are significant. Alternatively, pseudo-bidomain formulations can be used, combining a monodomain model with an infrequent bidomain solve to obtain full extracellular potential (Φ_e) distributions, and traces. However, previous attempts at such approaches did not see the expected significant decrease in compute time and did not include important effects of bath-loading on activation wavefront morphology (present in full bidomain models), representing a less accurate source term for Φ_e solution. ECG traces can also be derived from computationally cheaper Φ_e recovery techniques, whereby the time-course of Φ_e is approximated at a particular point using the monodomain transmembrane potential as source term. However, Φ_e recovery methods also assume tissue to be immersed in an unbounded conductive medium; not the case in most practical scenarios. We recently demonstrated how bath-loading effects in bidomain simulations could be replicated using an augmented monodomain model, faithfully reproducing bidomain wavefront shapes and activation patterns. Here, a computationally-efficient pseudobidomain formulation is suggested which combines the advantages of an augmented monodomain method with an infrequent bidomain solve, providing activation sequences, ECG traces and Φ_e distributions in a bounded medium surrounding the heart which closely match those of the full bidomain, but at $\approx$10% the computational cost. We demonstrate the important impact of both bath-loading and a finite surrounding bath on spatiotemporal Φ_e distributions, thus demonstrating the utility of our novel pseudobidomain model in ECG computation with respect to previous pseudobidomain and Φ_e recovery approaches.**

***Index Terms*—Augmented monodomain, Bidomain model, ECG, extracellular potential.**

I. Introduction

THE steep increase in available compute power in recent years, along with remarkable advances in computational modelling and medical imaging, have rendered the use of personalized multiscale computer models of electrophysiological function at the organ scale feasible. Such *in silico* models are poised to open new perspectives for novel clinical and industrial applications, such as optimization of therapy planning and delivery [1], or assessment and prediction of drug actions [2]. Despite the wide variety of potential applications of these models however, the majority of uses share the common need for computing realistic electrocardiograms (ECG), owing to its omnipresence in assessing cardiac function.

Over the past few years, major methodological efforts have been invested to integrate a rapidly growing wealth of experimental data into mechanistic models, in pursuit of the objective to minimize differences between *in vitro/in vivo* observations with *in silico* results by accounting for more and more subtle biophysical details. For example, high-resolution imaging datasets have been used to represent fine-scale details of cardiac anatomy at paracellular resolution [3]–[5], generating immensely structurally-complex models. Considering the substantial costs involved in developing such complex models, it comes as a surprise that modelling of the ECG, despite its central clinical importance, relies on fairly simple methodology. Most previous studies employed a monodomain approach, where ECG traces were computed using Φ_e recovery techniques [6], [7], where the time-course of the extracellular potential is approximated at a single point in space using the transmembrane potential from the monodomain model as the bioelectric source, involving a number of inherent physical approximations to the system. Although the monodomain model is a fairly good source model when approximating electrical activity of tissue immersed in a nonconducting medium (i.e., tissue exposed to air), its ability in accounting for the feedback effects of extracellular potentials upon depolarization and repolarization in the presence of a bath, is of limited accuracy. Moreover, most studies employed Φ_e recovery techniques where the underlying formalism relied upon the simplifying assumptions of tissue being immersed in an unbounded conductive medium; however, this is not the case in most, if not all, scenarios of practical relevance: cardiac tissue is virtually always immersed in a homogeneous bounded volume conductor, where the boundaries interfere with the extracellular field evoked by the cardiac sources. This weakness can be tackled by employing more elaborate recovery techniques based on the boundary element method, which do correctly predict the influence of a bounded volume conductor and conductive heterogeneities in the tissue [8].

As a consequence, the bidomain model, which explicitly considers current flow in both intra- and extracellular domains, is the preferred approach due to its capability to faithfully predict

Manuscript received March 4, 2011; revised April 4, 2011; accepted April 22, 2011. Date of publication May 2, 2011; date of current version July 20, 2011. The work of M. Bishop was supported by the Wellcome Trust through a Sir Henry Wellcome Postdoctoral Fellowship. The work of G. Plank was supported by the Austrian Science Fund FWF under Grant F3210-N18. *Asterisk indicates corresponding author.*

M. J. Bishop is with Computing Laboratory, University of Oxford, Oxford, OX1 3QD, U.K. (e-mail: martin.bishop@comlab.ox.ac.uk).

*G. Plank is with the Institute of Biophysics, Medical University of Graz, Graz, Austria, and also with Oxford e-Research Centre, University of Oxford, Oxford, OX1 3QD, U.K. (e-mail: gernot.plank@medunigraz.at).

Color versions of one or more of the figures in this paper are available online at http://ieeexplore.ieee.org.

Digital Object Identifier 10.1109/TBME.2011.2148718

the ECG. However, bidomain simulations are computationally quite expensive. Typically, the incurring computational costs exceed those of a monodomain approach by a factor of 10 [4], which preclude its application in those scenarios where very fast simulation-analysis cycles are key. An elegant approach to combine the advantages of the lower computational expenses of a monodomain with the superior capabilities of the bidomain in computing the ECG was reported by Potse *et al.* (2006) [9]. To save computation time, Φ_e was computed infrequently at a prescribed output resolution by performing additional solves of the elliptic portion of the bidomain. That is, the number of elliptic solves, which is computationally the most expensive operation in any bidomain simulation, could be reduced by more than an order of magnitude. Nonetheless, the computational savings were rather moderate: approximately a factor of 2 faster than full bidomain. Although this formalism correctly accounts for boundary effects in the volume conductor, the source model is monodomain and as such it neglects potentially very important bath-loading effects which are known to increase conduction velocity along tissue surfaces, inducing wavefront curvature [6], [10], [11]. As we have demonstrated in a previous study [12], the impact of bath-loading on wavefront profiles can be, depending on the chosen set of conductivity values, substantial, but by applying a careful augmentation approach, monodomain models can replicate the same wavefront profiles as in the fullblown bidomain, at a significantly lower computational expense.

The goal of this study is to present a computationally efficient pseudobidomain model of cardiac electric activity providing all relevant bidomain quantities at a fraction of the computational cost. The main novelty in this method is through the combination of an augmented monodomain approach to accurately simulate V_m activation sequences and wavefront morphologies (including bath-loading effects), along with an infrequent solve of the elliptic portion of the bidomain equations to faithfully reproduce the clinically-relevant ECG and full Φ_e distribution within a bounded medium surrounding the heart. Further novelty lies in the method's significantly greater computational speed-up relative to full bidomain, compared to previous pseudobidomain approaches [9]. We assess the accuracy of our novel pseudobidomain model in faithfully reproducing both spatial distributions and activation sequences of Φ_e and V_m, relative to the "gold standard" fullblown bidomain model, as well as temporal ECG traces, demonstrating its advantages over Φ_e recovery methods. We highlight the important role played by the augmentation approach, which can lead to large differences in accuracy relative to previous approaches [9]. Finally, we demonstrate significant increases in computational speed of our pseudobidomain, relative to full bidomain, model ($\sim 10\times$ faster) and provide an explanation of the implementation factors responsible for this difference.

II. Methods

A. Bidomain Formulation

The bidomain equations state that transmembrane currents, I_m, that enter intracellular and extracellular spaces by crossing the cell membrane, represent sources for intracellular, Φ_i, and extracellular, Φ_e, potentials and are given by

$$\nabla \cdot \boldsymbol{\sigma}_i \nabla \Phi_i = \beta I_m \tag{1}$$

$$\nabla \cdot \boldsymbol{\sigma}_e \nabla \Phi_e = -\beta I_m - I_{ei} \tag{2}$$

$$I_m = C_m \frac{\partial V_m}{\partial t} + I_{\text{ion}}(V_m, \boldsymbol{\eta}) - I_s \tag{3}$$

$$\nabla \cdot \sigma_b \nabla \Phi_e = -I_{eb} \tag{4}$$

where $V_m = \Phi_i - \Phi_e$ is the transmembrane voltage, $\boldsymbol{\sigma}_i$ and $\boldsymbol{\sigma}_e$ are the intracellular and extracellular conductivity tensors, respectively, β is the bidomain membrane surface to volume ratio, I_{ei} and I_{eb} are extracellular stimuli applied in the interstitial space or the bath, respectively, I_s is a transmembrane stimulus, C_m is the membrane capacitance per unit area, and I_{ion} is the membrane ionic current density which depends on V_m and a set of state variables $\boldsymbol{\eta}$.

Equations (1)–(4) can be recast and solved in the elliptic-parabolic form given by

$$\begin{bmatrix} -\nabla \cdot (\boldsymbol{\sigma}_i + \boldsymbol{\sigma}_e) \nabla \Phi_e \\ -\nabla \cdot \sigma_b \nabla \Phi_e \end{bmatrix} = \begin{bmatrix} \nabla \cdot \boldsymbol{\sigma}_i \nabla V_m + I_{ei} \\ I_{eb} \end{bmatrix} \tag{5}$$

$$\beta C_m \frac{\partial V_m}{\partial t} = (\nabla \cdot \boldsymbol{\sigma}_i \nabla \Phi_i) - \beta \left(I_{\text{ion}}(V_m, \boldsymbol{\eta}) - I_s \right). \tag{6}$$

At tissue boundaries, no flux boundary conditions are approximated for Φ_i, as well as continuity of Φ_e and the normal component of the extracellular current. At the boundaries of the conductive bath surrounding the tissue, no flux boundary conditions for Φ_e are imposed. The full bidomain model thus provides the most physiologically realistic representation of cardiac bioelectric activity, giving full V_m and Φ_e distributions at every point in space and time (typically 5–50 μs depending upon the application), as well as implicitly accounting for the effects of bath-loading upon wavefront dynamics through representation of a surrounding extracellular bath [12].

B. Augmented Monodomain Formulation

Assuming that the intra- and extracellular domains are anisotropic, but to the same degree, the bidomain equations can be reduced to the monodomain equation, allowing the cardiac tissue to be represented as a single conducting domain. Such a simplification assumes that $\boldsymbol{\sigma_e} = \lambda \boldsymbol{\sigma_i}$, where λ is a scalar. Substitution of this relation into (1) and (2), reduces the system to the monodomain equation

$$C_m \frac{\partial V_m}{\partial t} + I_{\text{ion}} = \nabla \cdot (\boldsymbol{\sigma_m} \nabla V_m) \tag{7}$$

where $\boldsymbol{\sigma_m}$ is the harmonic mean conductivity tensor or the effective *bulk conductivity*, which leads to an accurate match in conduction velocities between bidomain and monodomain formulations along the axial directions of the tissue. (For a full derivation see [12].)

As shown previously [12], activation patterns including bath-loading effects observed in bidomain models can also be faithfully reproduced with monodomain models in which

conductivity tensors are further carefully chosen. In this case, the harmonic mean conductivity tensor $\boldsymbol{\sigma_m}$ in (7) is represented by $\boldsymbol{\sigma_m^*}$, where the $*$ signifies either b in the tissue bulk or s along the surfaces. Considering propagation along individual principal axes, the eigenvalues of $\boldsymbol{\sigma_m^*}$ are given as

$$\sigma_m^{b\zeta} = \frac{\sigma_i^\zeta \sigma_e^\zeta}{\sigma_i^\zeta + \sigma_e^\zeta} \tag{8}$$

where $\zeta = l|t|n$ are the eigendirections of the tissue along the cardiac fiber direction ($\zeta = l$), transverse ($\zeta = t$) to the fibers within a sheet, and along a sheet normal direction ($\zeta = n$). A thin augmentation layer is defined by assuming that extracellular resistivity close to tissue surfaces is rather governed by the bath conductivity σ_b than the interstitial conductivity σ_e. Conductivity in the augmentation layer is then assumed to be

$$\sigma_m^{s\zeta} = \frac{\sigma_i^\zeta \sigma_b}{\sigma_i^\zeta + \sigma_b}. \tag{9}$$

The *augmented monodomain* approach thus faithfully reproduces the bath-loading effects of a surrounding extracellular medium (in terms of wavefront morphologies and conduction velocities) whilst, as it is just a monodomain model, only representing spatial and temporal changes in V_m [12].

C. Pseudobidomain Formulation

A pseudobidomain formulation is suggested here which combines the advantages of an augmented monodomain approach (providing the same activation sequence as bidomain, but at a much cheaper computational cost) with a fullblown bidomain (providing realistic ECG signals in a bounded medium surrounding the heart). In the case of the pseudobidomain, we combine the augmented monodomain representation along with an infrequent solve of the elliptic portion of the bidomain equations, which is only solved at those instances which correspond to a specified output granularity. That is, bioelectric activity in the heart is computed using (7) with augmented conductivities given by $\boldsymbol{\sigma_m^*}$, and Φ_e distributions throughout the domain are then computed by solving

$$\begin{bmatrix} -\nabla \cdot (\boldsymbol{\sigma}_i + \boldsymbol{\sigma}_e) \nabla \phi_e \\ -\nabla \cdot \sigma_b \nabla \phi_e \end{bmatrix} = \begin{bmatrix} \nabla \cdot \boldsymbol{\sigma}_i \nabla V_m \\ 0 \end{bmatrix}. \tag{10}$$

In the pseudobidomain formulation, V_m is computed at a timestep governed by the ODE system (5–50 μs, similar to full bidomain formulation), whereas Φ_e is computed at a desired output granularity, typically only at every 1 ms. Our pseudobidomain approach provides a faithful physical representation of the bath-loading effects upon activation dynamics (provided by the augmented monodomain model) as well as physically realistic spatial distributions of Φ_e from the elliptic part of the bidomain model. Note, that it is also possible to use a pseudobidomain approach which obtains V_m from a standard monodomain model lacking augmentation (using $\boldsymbol{\sigma_m}$ in (7) with conductivities given by (8) everywhere), as proposed by Potse *et al.* previously [9]. In this case, however, although Φ_e spatial distributions are obtained in a similar manner, the tissue-bath effect upon activation sequences is not accounted for [12]. Finally, we note that it is not possible to use the pseudobidomain approach to account for the effects of extracellular stimulation through I_{eb} or I_{ei} in (5).

D. Φ_e Recovery Method

Assuming that the tissue is immersed in an unbounded volume conductor, Φ_e can be recovered during a standard monodomain simulation by solving

$$\Phi_e = \frac{1}{4\pi\sigma_b} \int_\Omega \frac{\beta I_m}{\|\mathbf{r}\|} \, d\Omega \tag{11}$$

where $\mathbf{r}$ is the distance vector between source and field points. Using (7) the source term βI_m is given by $\nabla \cdot (\boldsymbol{\sigma_i} \nabla V_m)$. In this study V_m as computed by the augmented monodomain models was used, as this provides a more accurate representation of the bioelectric sources than a standard monodomain model.

E. Tissue Setup

A regular hexahedral finite element tissue model, with dimensions 1.0 cm $\times$ 0.01 cm $\times$ 0.5 cm in the x-, y-, and z-directions, respectively, and including a bath of initial thickness 0.1 cm in the z-direction surrounding the tissue, was generated with the meshing software Mesher. Tissue node discretization was 100 μm, giving a total of $14\,342$ nodes and 7000 elements. Cell membrane dynamics within the myocardial tissue were represented by the modified Beeler–Reuter rabbit ventricular cell model [13], which models the total transmembrane current, I_m. Conductivities along the fiber (l) and cross-fiber (t, n) directions within the intracellular (g_i^l, $g_i^{t,n}$) and extracellular (g_e^l, $g_e^{t,n}$) domains were defined by previously experimentally measured values from the literature [14] of $g_i^l = 0.34$, $g_i^t = 0.060$, $g_e^l = 0.12$, and $g_e^t = 0.080$. Such values are chosen as they have recently been shown to induce a significant bath-loading induced curvature to the activation wavefront [12]. The default value of the conductivity of the extracellular bath (g_b) was set to 1.0 S/m (isotropic).

In addition to the slab model, a recently published high-resolution MRI-derived rabbit ventricular finite element model [3] was also used. The model contains $\sim$4 million myocardial nodes points, constituting $\sim$24 million tetrahedral elements (mean element edge-length $\sim$130 μm), and sits within a perfusing bath surrounding the ventricles and filling all cavities. The model represents ventricular myocardial tissue, containing intra-myocardial blood vessels and cleft spaces as well as endocardial structures within the ventricular cavities, as detailed in [3]. The extracellular potential Φ_e was fixed at a node in the bath (see Fig. 1, green circle).

F. Stimulation Protocol

The slab model was paced through application of a transmembrane current pulse of 0.005 μA/cm^3 over 1 ms duration along the $x = 0$ plane of the tissue to elicit propagation in the x-direction. For the whole ventricular model, the pacing stimulus was applied to the apex of the ventricles. Identical protocols were repeated in both models with electrical activity simulated

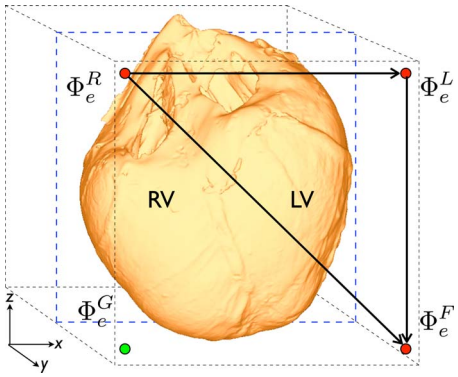

Fig. 1. Clinical 3-lead ECG calculation on the whole-ventricular rabbit model. Black dashed box shows extent of surrounding extracellular bath; blue dashed plane shows clipping-plane used for analysis in Fig. 6.

using three methods: BDM—fullblown bidomain model using (5) and (6); PBA—pseudobidomain model using (7) with augmentation of conductivities $\boldsymbol{\sigma}_{\boldsymbol{m}}^{*}$ (defined by (8) in the bulk and (9) within the surface augmentation layer) along with (10); and, PB—pseudobidomain model using (7) without augmentation $\boldsymbol{\sigma}_{\boldsymbol{m}}$ (defined only by (8) everywhere) along with (10) as proposed previously [9].

G. Computation of Φ_e and ECG Traces

Extracellular potential traces are computed either as unipolar electrograms, i.e., the potential difference between Φ_e at a recording site and a chosen reference potential in the case of BDM, PBA, or PB, or, in the case of a monodomain model, a zero reference potential in an unbounded bath, which is implicitly assumed when using Φ_e recovery method. ECG traces are computed as bipolar extracellular electrograms by subtracting two unipolar electrograms. For the whole ventricular model, ECG traces as measured with an Einthoven configuration are approximated by a lead configuration as shown in Fig. 1. Bath dimensions surrounding the ventricles in Fig. 1 are 23.9 mm, 22.0 mm, and 33.0 mm in the x-, y- and z-directions, respectively. The green circle represents the zero reference potential, approximating the location of the right-leg used clinically, having potential $\Phi_e^G = 0$ always. Φ_e^L, Φ_e^R, Φ_e^F refer to the potentials measured at the left-arm, right-arm and left-leg (or foot), respectively. The Einthoven lead I, II and III recordings are calculated as $V_I = \Phi_e^L - \Phi_e^R$, $V_{II} = \Phi_e^F - \Phi_e^R$, and $V_{III} = \Phi_e^F - \Phi_e^L$, respectively.

H. Comparing Φ_e Recovery and Pseudobidomain-Derived ECG Traces

The Φ_e recovery approach relies upon the assumption that the bioelectric sources are immersed in an unbounded homogeneous volume conductor. However, in a real-world scenario this is never the case. A surrounding medium is always of limited size and is never homogeneous, where both factors influence the distribution of Φ_e in the volume conductor which is also reflected in the morphology of both unipolar electrogram and ECG traces. To assess the dependency of Φ_e traces upon bath volume the pacing protocol of Section III-B was repeated with the PBA method upon a series of adapted models, of the same tissue dimensions, but with a varying volume of bath surrounding the tissue. The model set-ups, shown in Fig. 5 (top panel), included:

1) 1 mm of bath surrounding the tissue on each side in the z-direction (default tissue-bath set-up);
2) 5 mm of bath surrounding the tissue on each side in the z-direction;
3) 1 mm of bath surrounding the tissue on each side in both the z- and y-directions;
4) 5 mm of bath surrounding the tissue on each side in both the z- and y-directions.

I. Computational Considerations

The bidomain equations were solved with the Cardiac Arrhythmia Research Package (CARP) [15]. The specifics of the numerical regimes used in CARP have been described extensively elsewhere [15]–[18]. Visualization of results was performed with the custom written Meshalyzer software (Courtesy of Dr. E.J. Vigmond).

III. Results

A. V_m and Φ_e Distributions in a Slab Model

Of utmost importance in any model aiming to replicate a full bidomain representation is the faithful simulation of both V_m and Φ_e distributions in space and time, both within the tissue and the surrounding bath. Fig. 2 plots V_m (column 1) and Φ_e (columns 3) distributions with the tissue slab and Φ_e distributions within the entire domain 17.5 ms following the pacing stimulus for simulations performed with the BDM (top), the PBA (centre), and the PB (bottom). Shown also is an activation map of V_m (column 2).

Fig. 2 clearly shows that the PBA provides a very close match to the BDM both in terms of V_m activation sequences and wavefront morphologies within the tissue, as well as Φ_e distributions within and surrounding the tissue. Quantitatively, conduction velocities were similar in both models, with the node shown in Fig. 2 (red circle in PB panel) being depolarized at 17.0 ms in the BDM case, compared to 17.5 ms for the PBA. Only very minor differences exist in the profile of the wavefront (evident in the activation maps), with the BDM predicting a full V-shaped wavefront, compared to the PBA which predicts a V-shape with slightly flattened regions close to the surface. In addition, slight differences are also seen in the Φ_e isocontour shapes close to the upper ($x = 1$ cm) tissue boundary. However, it is noted that the PB predicts very different wavefront profiles and Φ_e distributions compared to the BDM and PBA, specifically, showing a planar wavefront due to the absence of tissue-bath effects within the PB representation. Consequently, the corner node is depolarized at 24.6 ms in the PB model, showing a reduction in conduction velocity of approximately 40–45% compared to the BDM/PBA cases. Movies of V_m and Φ_e dynamics can be found in the Supplementary Information.

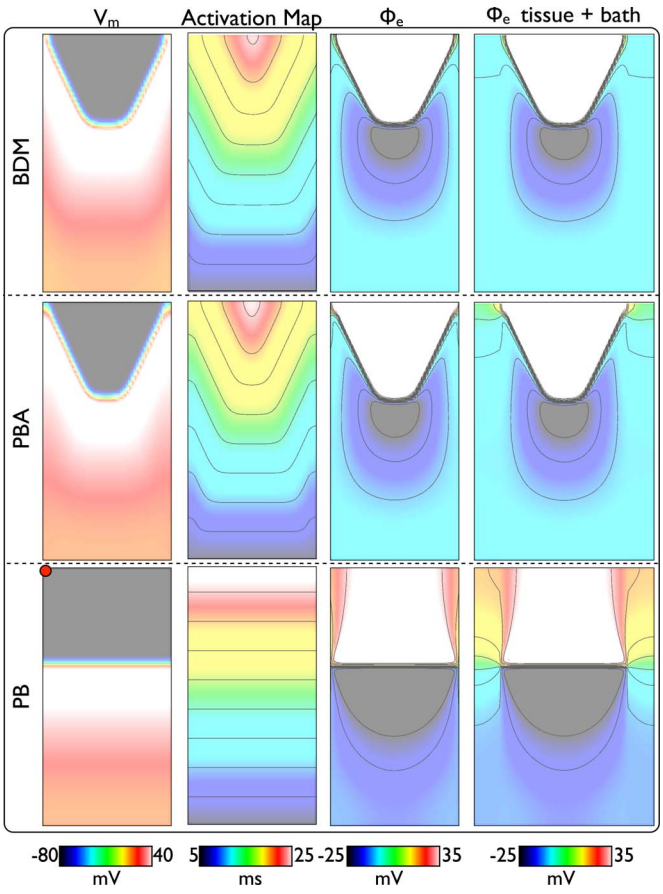

Fig. 2. V_m and Φ_e distributions within the tissue, and Φ_e distribution within the entire domain (tissue plus bath), at 17.5 ms, for the BDM (top), PBA (center), and PB (bottom) models. Also shown is a V_m activation map. Note, black/white correspond to the minimum/maximum of the color-bar scale.

Computationally, the full 300 ms simulations with an ODE time-step of 5 μs took $457/460$ s for the PBA/PB models on four 2.66 GHz Intel Xeon CPUs, compared to 4526 s for the BDM model. Of the total simulation time, $18.3/18.5\%$ was spent on the elliptic solve in the PBA/PB, compared to 89.3% for the BDM model.

B. Unipolar Φ_e Traces in a Slab Model

Fig. 3 compares Φ_e traces from nine separate locations within the domain for the BDM (red dashed line), PBA (blue solid line) and PB (green dotted–dashed line) models. Observation points are selected at the extremity of the bath (1–3) 1 mm from the tissue surface, at the tissue–bath interface (4–6) and within the bulk of the tissue (7–9).

Fig. 3 shows that, for all locations, the PBA gives very similar Φ_e traces to the BDM, closely matching it both during depolarization and repolarization phases. During depolarization, the PBA traces predict amplitudes with magnitudes less than 1.6 mV different to those of the BDM traces, and less than 0.6 mV during repolarization. However, the time of maximum depolarization of the PB Φ_e traces is seen to lag those of the PBA and BDM traces, with an increasing lag further from the stimulus site due to the previously noted faster conduction velocities of the PBA and BDM model (Fig. 2) due to bath-loading effects. Furthermore, the differences in activation wavefront morphology of the PB relative to the PBA and BDM seen in Fig. 2 are also seen to translate into different Φ_e trace morphologies here: the PB model generally appears to predict larger positive depolarization inflections (QR), and consistently over-estimates the amplitude of the repolarization T-wave relative to the PBA and BDM. In this case, the PB model predicts trace amplitudes with magnitudes up to 10.4 mV different to those of the BDM model, and up to 1.8 mV during repolarization.

C. V_m and Φ_e Distributions and Einthoven 3-Lead ECG in a Whole Ventricular Model

Fig 4(left) shows V_m and Φ_e distributions within the ventricular myocardium 40 ms following application of an apical stimulus to the model for the BDM (top row), PBA (center row), and PB (bottom row). In the third column, we show the Φ_e distribution within the full 3D volume of the model, i.e., within both the ventricular myocardium and the extracellular bath (including bath within the cavities, blood vessels and surrounding bath).

Again, the PBA model faithfully replicates the activation wavefront morphologies and spatial/temporal potential distributions predicted by the BDM model on this anatomically-complex model, whilst the match with the PB is less close. Quantitatively, the time taken for the depolarization wavefront to reach the node (red circle in PB panel) is 61.4 and 61.5 ms in the BDM and PBA models respectively, compared to 79.8 ms in the PB case, replicating the reduced conduction velocity witnessed in Fig. 2 due to the absence of bath-loading effects in the PB model.

Using the lead configuration as shown in Fig. 1, Einthoven-lead I, II, and III recordings were computed. Resulting ECG traces are shown in Fig. 4 (right) for BDM (red dashed line), PBA (blue solid line), and PB (green dotted–dashed line). Again, we see how the traces derived from the PBA and the BDM models are almost visually indistinguishable. However, in comparison, the PB traces differ significantly, with maximum trace amplitudes differing by up to 1.24 mV (76%) during depolarization and 0.38 mV (123%) during repolarization, compared to the BDM model, and the timing of depolarization occurring up to 16 ms following that of the BDM. Computationally, a similar speed-up was witnessed as in the case of a simple slab model, with the compute times of the PBA/PB being a factor of ~ 10 times faster than the BDM simulation.

D. Comparison With Φ_e Recovery Method

Φ_e traces can be derived directly from monodomain simulations (potentially also including the effects of augmentation) via the Φ_e recovery method, described in Section II-D. Overall, this technique is very widely used due to its reduced complexity as compared to bidomain or pseudobidomain approaches and its significantly lower computational costs, particularly if Φ_e has to be recovered at a very limited number of observation sites. To investigate under which circumstances this method is suitable for the simulation of ECG traces we compared the accuracy of

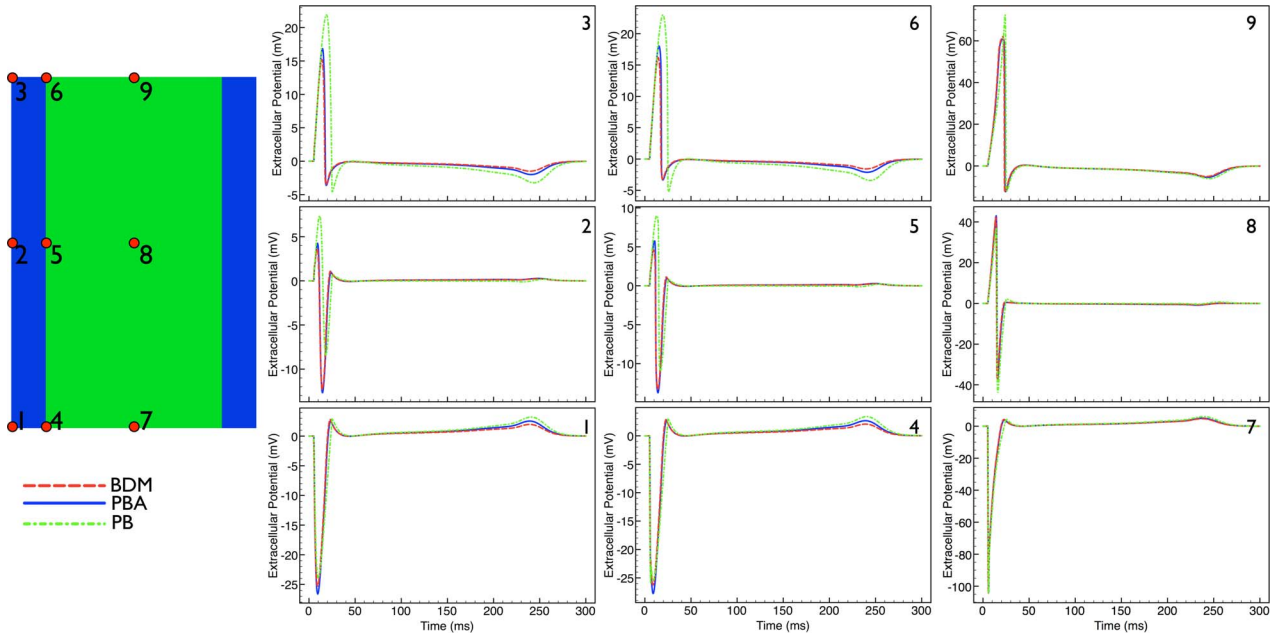

Fig. 3. Comparison of Φ_e traces taken from nine different locations within the domain (shown left) for BDM (red dashed line), PBA (blue solid line), and PB (green dot-dashed line).

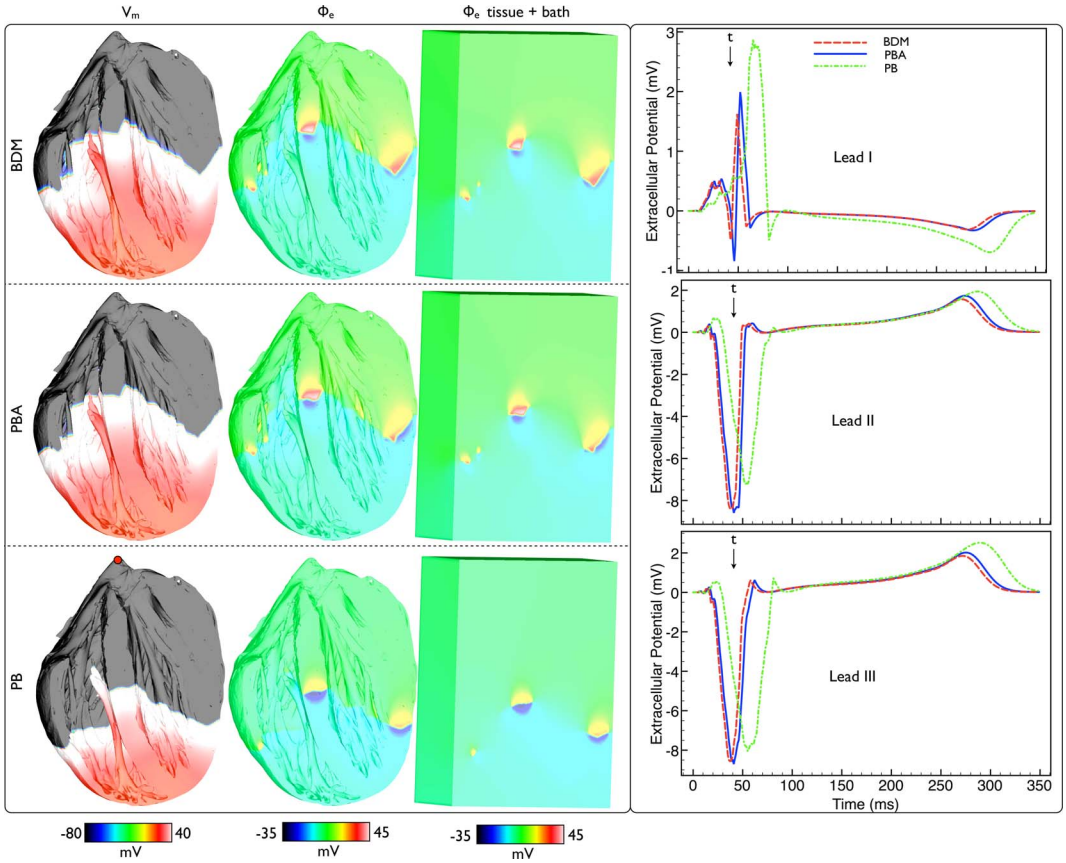

Fig. 4. Application of the pseudobidomain approach to a whole rabbit ventricular model. *Left:* V_m and Φ_e distributions within the tissue, and Φ_e distribution within the entire domain (tissue plus bath), at 40 ms following apical stimulus, for the BDM (top), PBA (center), and PB (bottom) models within the whole-ventricular model, with clipping planes used to expose endocardial surfaces/structures. Here, the clipping-plane (shown in Fig. 1) is used to expose intra-myocardial and intra-cavity potential data. Note, black/white correspond to the minimum/maximum of the color-bar scale. *Right:* 3-lead ECG traces, calculated as detailed in Fig. 1, for the BDM (red dashed line), PBA (blue solid line) and PB (green dotted–dashed line). Time marked *t* in ECG traces shows time corresponding to potential distributions.

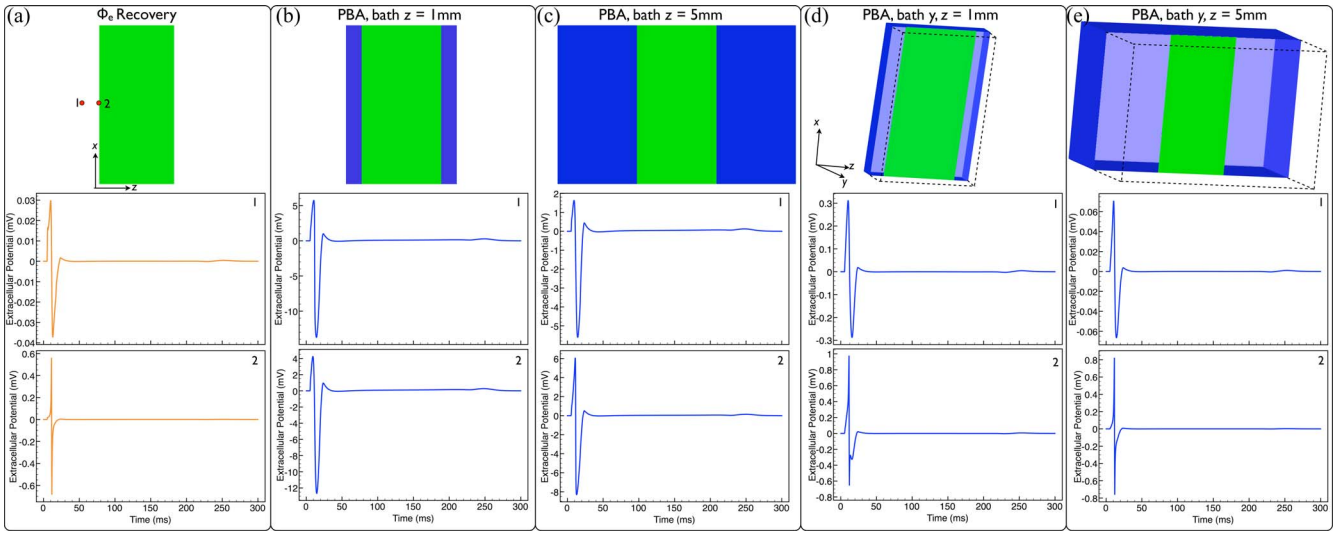

Fig. 5. Comparison of Φ_e electrogram traces from Φ_e recovery and PBA methods for differing volumes of surrounding baths. (a) Φ_e traces (orange) from Φ_e recovery method obtained from points 1 (1 mm from tissue surface) and 2 (on tissue surface) which assumes the tissue is surrounded by an infinite bath in all dimensions. (b)–(d) Φ_e traces (blue) from PBA method from points 1 and 2 with models containing 1 mm (b) and 5 mm (c) bath surrounding the tissue on each side in the z-direction, and (d) 1 mm and (e) 5 mm bath in z- and y-directions, respectively.

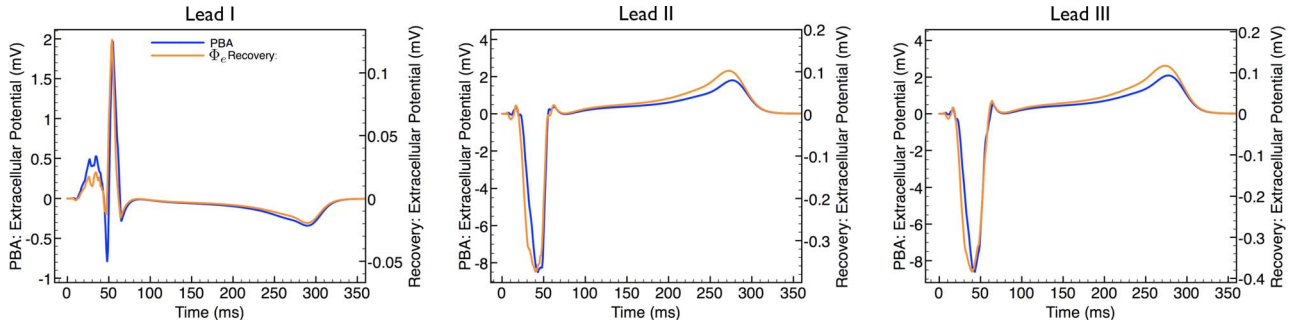

Fig. 6. Accuracy of the Φ_e recovery method applied to whole rabbit ventricular models. 3-lead ECG traces, calculated as detailed in Fig. 1, for the PBA (blue traces) and the Φ_e recovery method (orange traces).

the Φ_e recovery method relative to the pseudobidomain method and how this depends upon factors such as recording location and the volume of surrounding bath modeled.

1) Dependence Upon Bath Volume: Using the slab model immersed in a bath of varying volume, Φ_e uni-polar electrogram traces were computed by employing either the PBA method, shown in Fig. 5(b)–(d), or the Φ_e recovery method using the V_m output of the PBA method, shown in Fig. 5(a) (orange traces) which assumes the tissue is surrounded by an infinite homogeneous bath in all dimensions. Note, however, that Φ_e traces as computed with the Φ_e recovery technique do not depend upon bath volume, but only upon a given V_m computed in the absence of a bath; thus, only one set of Φ_e traces from the Φ_e recovery method is shown.

Overall, the time-course of the Φ_e traces predicted by the Φ_e recovery method and calculated directly with the PBA method are similar. However, evident from the PBA (blue) traces of Fig. 5 is that, for small volumes of bath surrounding the tissue, the trace amplitude of the Φ_e recovery method is significantly smaller than that given by the more physiologically realistic PBA method, with this difference being accentuated with distance from the tissue. However, as the bath volume increases, the amplitudes of the PBA traces significantly decrease, and become of the same order of magnitude as those predicted by the Φ_e recovery method. Furthermore, comparing panel (b) with both (c) and (d) of Fig. 5 we note that adding bath in an additional dimension (y) has a larger impact on the trace amplitude than simply increasing the bath in the z-direction, as in the former case the *volume* of bath surrounding the thin tissue slice increases by relatively a much greater degree. In addition, the asymmetry in the positive/negative inflections of the Φ_e traces for the PBA method become more symmetrical (in-line with the Φ_e recovery method) for larger bath volumes surrounding the tissue. Thus, only for large bath volumes do the PBA and Φ_e recovery traces achieve similar results.

2) Differences With Whole-Ventricular Models: Fig. 6 compares Einthoven-like ECG traces (calculated as detailed in Fig. 1) obtained from the whole rabbit ventricular model for the Φ_e recovery method (orange traces, right axes) and the PBA method [blue traces, left axes repeated from Fig. 4 (right)]. The Figure shows that, as in the case of the aforementioned simple slab model, the overall time-course of the ECGs are similar

between the two methods. However, as before, the amplitudes of the traces again differ considerably, with the ECG traces predicted by the Φ_e recovery method consistently underestimating both the positive and negative depolarization amplitudes of the PBA method traces by over an order of magnitude. Although, in this case, we have a bath extending in all 3-D, the volume of tissue represented by the ventricles is quite large relative to the surrounding bath, which only extends a few millimetres from the tissue surface in places (see Fig. 1). Thus, the Φ_e recovery approximation (which assumes an infinite bath) does not hold as true as in Fig. 5(e) where the relative tissue-to-bath volume ratio is a lot lower.

IV. Discussion

In this study, a novel pseudobidomain approach based on using an augmented conductivity tensor (PBA) is presented which offers a number of distinct advantages over fullblown bidomain models or the use of monodomain formulations coupled to forward models to predict Φ_e distribution and ECG traces. The PBA approach matches very closely both V_m and Φ_e distributions as they are observed in a bidomain model. Although the complexity in terms of memory costs and required solver technology is the same as in the case of a bidomain, pseudobidomain simulations (both PBA and PB) are executed at the speed of a monodomain simulation. That is, the pseudobidomain approach provides results which are virtually indistinguishable from bidomain results, but at a fraction of the computational costs, resulting in performance gains of about an order of magnitude.

A. Improved Representation of Bioelectric Sources

As previously demonstrated [12], using an augmented monodomain formulation allows the accurate representation of V_m activation sequences, including wavefront acceleration and curvature induced by bath-loading. Such an improved representation of cardiac biolelectric sources is key for biophysically accurate simulations of extracellular Φ_e distributions and ECG traces. As we have demonstrated here, not representing bath-loading effects can lead to up to a 45% difference in conduction velocity and substantial differences in V_m and Φ_e activation wavefront morphologies (see Figs. 2 and 4), which together translate into differences in electrogram morphology, amplitude and timing (see Figs. 3 and 4). Such differences could be imperative in the developing use of simulated ECGs in the prediction of anti-arrhythmia drug efficacy where accurate simulation of such biomarkers is essential [2]. This is in line with previous observations, where simulations using a "dry" heart, i.e., where the heart is not immersed in a conductive medium, led to Φ_e predictions which were outside the physiological range [9]. To arrive at realistic prediction of ECG traces the ventricular cavities had to be filled with blood and a bath layer of 1 mm thickness had to be added to the epicardium. Although Potse *et al.* reported a good match between their bidomain simulations and their monodomain model without augmentation (referred to as PB in this study), insights gained in this study rather suggest that there are noticeable differences due to two main factors: Firstly, a plain monodomain model, as used in their study, cannot account for the presence of a surrounding conductive medium, and as such the impact of bath-loading induced changes in source distribution upon predicted Φ_e distributions and ECG traces remain unaccounted for. Thus, the PBA model developed here represents an imperative improvement upon previous studies presenting a monodomain approach which also used an infrequent bidomain solve to derive Φ_e [9]. Secondly, in contrast to the claim in Potse *et al.*, monodomain simulations using bulk conductivities do not produce the exactly same activation patterns as bidomain simulations, not even in the absence of a bath [19], [20]. However, these differences are very subtle and as such they are very unlikely to have any significant impact on ECG morphology.

B. Computational Costs

In terms of execution time, a pseudobidomain simulation is only marginally more expensive than a monodomain simulation. This is due to the significantly reduced number of elliptic solves required which tends to be the computationally most expensive portion of a bidomain simulation [4]. Typically, due to accuracy constraints (7) is solved using time-steps in the range between 5 and 50 μs, whereas ECGs are typically sampled at a time-step of 1 ms. Hence, a full bidomain simulation requires roughly 20–200 times the number of elliptic solves of a pseudobidomain which suggests that substantial savings in execution time can be expected when using the PBA formulation. For instance, in [4], where the same whole ventricular rabbit model was used as in this study, between 82.9% and 90.5% of the overall execution time was attributable to solving the elliptic PDE. Similarly, in the simpler BDM slab model used here, 89.3% was spent on this endeavor.

Performance measurements conducted in this study clearly confirm that computational savings gained from a PBA approach are indeed significant. In the slab model, we observed a speed-up of roughly a factor of 10 when using the PBA instead of the BDM; in the whole ventricular model, the PBA (and PB) model was also seen to perform approximately ten times faster, replicating the speed-up witnessed in the simple slab model. Such computational savings when requiring the simulation of bidomain parameters (Φ_e distributions, ECGs) will have a significant impact in large scale (whole heart/torso), patient-specific simulations within the backdrop of time constraints within a clinical environment [1].

These significant speed-ups are in stark contrast to the rather moderate gains observed by Potse *et al.* [9] where only a reduction by a factor of 2 in execution time was achieved. Reasons for this discrepancy are likely to be multifactorial, with candidate causes including the spatial discretization method (finite difference versus finite element method), problem size (26 million versus 9 million nodes), time step ($50/100$ μs versus 5 μs), memory model (shared versus distributed memory), implementation details and the employed linear solver technique. According to their report, 74% of the overall execution time during fullblown bidomain was spent on solving the elliptic PDE, whereas in our study this percentage was higher, around 90%. That is, the potential speed-up in their implementation is limited

to less than a factor of 4. A further critical factor, in our view, is the choice of linear solver. Potse *et al.* employed an ILU (incomplete lower upper) preconditioner for a BiCGStab iterative solver. The weaknesses of such standard iterative methods are very well known and understood [21]. These methods are inefficient in removing the low-frequency components of the residual which slows down convergence after the high-frequency components are removed from the residual during the first few iterations. These insights motivated the development of multigrid methods which project residuals onto a coarser space where low-frequency components are dealt with in a more efficient manner. The superiority of multigrid methods in the context of the bidomain equation has been demonstrated in previous studies [16], [22]. A key factor seemed to be the dependency of their solver strategy upon the initial guess. According to their report, using the previous time-step as an initial guess reduced the number of iterations required for convergence by two orders of magnitude. In the PB case, however, the quality of this initial guess must degrade substantially, since the previous elliptic solve available lags the sought after solution by 1 ms. Therefore, although not explicitly reported, the lack of a good initial guess may have led to a significant increase in the number of iterations, thus preventing them fully exploiting the potential benefits of a reduced number of elliptic solves.

On the other hand, in our study we employed an algebraic multigrid solver [16] which always converged to a tolerance of 10^{-9} of the unpreconditioned residual within less than 9 iterations. This method is not overly sensitive to the choice of an initial guess. As reported in an earlier study [16], even when using a zero initial guess, iteration numbers increased only moderately by a few percent. This is confirmed in this study where the average number of iterations increased only marginally, from 7.7 iterations in the BDM case to 9.8 iterations in the PBA case. Further, the fast convergence of our elliptic solver set-up allowed us to use the same stringent convergence criterion in all scenarios throughout this study, unlike in the study of Potse *et al.* where the convergence criteria had to be adjusted as a function of electrical state of the tissue to save compute time.

In terms of memory costs, the pseudobidomain is more expensive than a full bidomain since the additional stiffness matrix associated with σ_m^* is required. However, for parallel execution of simulations, memory costs are a lesser concern, since more compute cores can be added to increase available address space. In theory, this drawback could be avoided by repopulating the data structures used for storing the intracellular stiffness matrices associated with σ_i, however, extra compute time would incur, thus reducing achievable speed-up.

C. Accuracy of the Φ_e Recovery Method

In those cases where the full Φ_e distribution throughout the domain is not required, the Φ_e recovery method is frequently used in conjunction with monodomain simulations to obtain temporal ECG traces from particular locations. If combined with augmentation of the conductivities at the tissue surface to replicate the bath-loading effect [12], the more subtle bath-loading induced effects are reflected in recovered ECG traces. The remaining key limitation in the Φ_e recovery approximation lies in the assumption that the tissue is immersed in an infinite bath in all directions. We have demonstrated in this study that the effects of such an assumption lead primarily to differences in the magnitude of the ECG amplitude between the Φ_e recovery method and bidomain approaches, although the time-course of ECG traces were seen to still match closely. As the volume of bath surrounding the tissue in the bidomain model gets smaller in relation to the volume of tissue, ECG amplitudes increase, as the same amount of extracellular current (whose source is the tissue) is being shunted through a smaller region, increasing the current density and thus the voltage drop in the volume conductor. A close match in the ECG amplitude between the Φ_e recovery method and bidomain approaches is thus obtained in the presence of a large bath surrounding the tissue in all directions during a bidomain simulation relative to the volume of tissue (which controls the strength of the current source), as in Fig. 5(e).

However, in many practical scenarios the heart is often surrounded by a relatively small volume of bath, particularly in the *ex vivo* Langendorff bath-perfused optical mapping experiment, for example, represented by Fig. 1. We have shown in Fig. 6 that in such cases, although the Φ_e recovery method closely predicts the same ECG time-course as bidomain approaches, it still under-estimates the depolarization amplitude by over an order of magnitude. Therefore, in cases where accurate knowledge of the ECG amplitude is of direct relevance, it is thus unsuitable to use Φ_e recovery methods, and the more accurate bidomain method, or pseudobidomain method presented here, is required.

The results from the whole-ventricular simulations of Fig. 6 provide a useful guide as to the applicability of the Φ_e recovery method in predicting ECG traces from the *in vivo* situation of the heart lying within the torso, suggesting the method might underestimate trace amplitudes in this case. However, although the heart is relatively close (a few millimetres) from the external chest cavity, meaning there is little bath between it and many of the ECG measurement locations, it also resides within a large volume represented by the entire body. It thus remains to be determined the extent to which the relative volume of cardiac tissue to surrounding 'bath' in this case affects the approximation of the Φ_e recovery method in faithfully predicting ECG amplitudes, requiring the performance of whole torso computational bidomain simulations.

D. Limitations of the Pseudobidomain

Although the pseudobidomain model closely approximates a full bidomain formulation and, as such, is very well suited to many applications, the formulation is not as general, and cannot be used to replace the bidomain when effects of external stimulation are investigated. As can be seen by comparing (10) with (5), in the pseudobidomain formulation in (10) the terms I_{eb} and I_{ei} are set to 0. This is an indication of the fact that extracellular stimulation effects, either evoked via I_{eb} or by imposing boundary conditions upon Φ_e, cannot be properly modeled, since the solution for Φ_e, obtained by solving (10), is not fed back into

the parabolic PDE. That is, the pseudobidomain is a pure forward model which correctly predicts Φ_e distributions, but any feedback of changes in Φ_e cannot be accounted for, other than bath-loading effects [12].

The pseudobidomain can be straightforwardly converted to a full bidomain formulation on the fly during a simulation run, allowing entire protocols (including extracellular current and voltage stimulation) to be simulated efficiently, with only minor modifications being required.

1) The parabolic (6) and (7) have to be swapped. In practice, the stiffness matrices $\mathbf{K_m}$ associated with σ_m^*, and $\mathbf{K_i}$ associated with σ_i are swapped in the parabolic solver and applied to Φ_i instead of V_m, respectively.
2) To account for external stimulation, either boundary conditions are applied to the left-hand side of (10) or extracellular current is switched on by replacing the 0 term on the right hand side of (10) with I_e.

All of the aforementioned operations, however, have to be implemented in a general solver regardless. Assuming that formulations are only switched between a certain lead time prior to external simulation, during and for a certain lag time after stimulation, the computational cost is negligible, except for the cost of enforcing Dirichlet boundary conditions. This step requires tampering with the matrix structure and storing the rows and columns of Dirichlet nodes to be able to undo the modifications when reverting back to the pseudobidomain mode. Particularly in parallel this requires careful implementation to enable a quick and seamless switching between execution modes. Explicit nulling of the I_e term is not necessary since $I_e = 0$ holds regardless in the absence of a stimulus.

V. Conclusion

In this study, we have presented a novel pseudobidomain model of cardiac electrical activation which can successfully compute ECGs, activation sequences and Φ_e distributions, including the effects of bath-loading induced wavefront curvature, with accuracy comparable to the fullblown bidomain model, but at ~ 10 times smaller computational cost. Although augmented monodomain approaches can be used in conjunction with Φ_e recovery methods to compute ECGs, we have shown in cases of a finite surrounding bath, such methods are often not appropriate, emphasizing the utility of our method.

Acknowledgment

The authors acknowledge the use of the computing resources provided by the Oxford Supercomputing Center (OSC).

References

[1] S. Nieder, G. Plank, P. Chinchapatnam, M. Ginks, P. Lamata, K. Rhode, C. Rinaldi, R. Razavi, and N. Smith, "Length-dependent tension in the failing heart and the efficacy of cardiac resynchronisation therapy," *Cardiovasc. Res.*, vol. 89, pp. 336–343, 2011.

[2] D. Noble, "Computational models of the heart and their use in assessing the actions of drugs," *J. Pharmacol. Sci.*, vol. 107, pp. 107–117, 2008.

[3] M. Bishop, G. Plank, R. Burton, J. Schneider, D. Gavaghan, V. Grau, and P. Kohl, "Development of an anatomically-detailed MRI-derived rabbit ventricular model and assessment of its impact on simulation of electrophysiological function," *Am. J. Physiol. Heart Circ. Physiol.*, vol. 298, pp. 698–718, 2010.

[4] G. Plank, R. A. B. Burton, P. Hales, M. Bishop, T. Mansoori, M. O. Bernabeu, A. Garny, A. J. Prassl, C. Bollensdorff, F. Mason, F. Mahmood, B. Rodriguez, V. Grau, J. E. Schneider, D. Gavaghan, and P. Kohl, "Generation of histo-anatomically representative models of the individual heart: Tools and application," *Phil. Trans. Roy Soc. A*, vol. 367, pp. 2257–2292, 2009.

[5] D. Hooks, K. Tomlinson, S. Marsden, I. LeGrice, B. Smaill, A. Pullan, and P. Hunter, "Cardiac microstructure: implications for electrical propagation and defibrillation in the heart," *Circ. Res.*, vol. 91, no. 4, pp. 331–338, 2002.

[6] R. Plonsey, C. Henriquez, and N. Trayanova, "Extracellular (volume conductor) effect on adjoining cardiac muscle electrophysiology," *Med. Biol. Eng. Comput.*, vol. 26, pp. 126–129, 1988.

[7] K. Gima and Y. Rudy, "Ionic current basis of electrocardiographic waveforms: A model study," *Circ. Res.*, vol. 90, pp. 889–896, 2002.

[8] G. Fischer, B. Tilg, R. Modre, G. J. Huiskamp, J. Fetzer, W. Rucker, and P. Wach, "A bidomain model based BEM–FEM coupling formulation for anisotropic cardiac tissue," *Ann. Biomed. Eng.*, vol. 28, no. 10, pp. 1229–1243, 2000.

[9] M. Potse, B. Dubé, J. Richer, A. Vinet, and R. M. Gulrajani, "A comparison of monodomain and bidomain reaction-diffusion models for action potential propagation in the human heart," *IEEE Trans. Biomed. Eng.*, vol. 53, no. 2, pp. 2425–2435, Dec. 2006.

[10] C. S. Henriquez, A. L. Muzikant, and C. K. Smoak, "Anisotropy, fiber curvature, and bath loading effects on activation in thin and thick cardiac tissue preparations: Simulations in a three-dimensional bidomain model," *J. Cardiovasc. Electrophysiol.*, vol. 7, pp. 424–444, 1996.

[11] B. J. Roth, "Effect of a perfusing bath on the rate of rise of an action potential propagating through a slab of cardiac tissue," *Ann. Biomed. Eng.*, vol. 24, pp. 639–646, 1996.

[12] M. J. Bishop and G. Plank, "Representing cardiac bidomain bath-loading effects by an augmented monodomain approach: Application to complex ventricular models," *IEEE Trans. Biomed. Eng.*, vol. 58, pp. 1066–1075, 2011.

[13] J. P. Drouhard and F. A. Roberge, "Revised formulation of the Hodgkin–Huxley representation of the sodium current in cardiac cells," *Comput. Biomed. Res.*, vol. 20, no. 4, pp. 333–350, 1987.

[14] D. E. Roberts and A. M. Scher, "Effect of tissue anisotropy on extracellular potential fields in canine myocardium in situ," *Circulation Res.*, vol. 50, pp. 342–351, 1982.

[15] E. Vigmond, M. Hughes, G. Plank, and L. Leon, "Computational tools for modeling electrical activity in cardiac tissue," *J. Electrocardiol.*, vol. 36, pp. 69–74, 2003.

[16] G. Plank, M. Liebmann, R. Weber dos Santos, E. J. Vigmond, and G. Haase, "Algebraic multigrid preconditioner for the cardiac bidomain model," *IEEE Trans. Biomed. Eng.*, vol. 54, no. 4, pp. 585–596, Apr. 2007.

[17] E. J. Vigmond, R. Weber dos Santos, A. J. Prassl, M. Deo, and G. Plank, "Solvers for the cardiac bidomain equations," *Prog. Biophys. Mol. Biol.*, vol. 96, no. 1–3, pp. 3–18, 2008.

[18] G. Plank, L. Zhou, J. L. Greenstein, S. Cortassa, R. L. Winslow, B. O'Rourke, and N. A. Trayanova, "From mitochondrial ion channels to arrhythmias in the heart: Computational techniques to bridge the spatio-temporal scales," *Philos. Transact. A Math. Phys. Eng. Sci.*, vol. 366, no. 1879, pp. 3381–3409, 2008.

[19] P. C. Franzone, L. F. Pavarino, and B. Taccardi, "Simulating patterns of excitation, repolarization and action potential duration with cardiac bidomain and monodomain models," *Math. Biosci.*, vol. 197, pp. 35–66, 2005.

[20] B. F. Nielsen, T. S. Ruud, G. T. Lines, and A. Tveito, "Optimal monodomain approximations of the bidomain equations," *Appl. Math. Comput.*, vol. 184, pp. 276–290, 2007.

[21] W. Briggs, V. Henson, and S. McCormick, *A Multigrid Tutorial*, 2nd ed. Philadelphia, PA: SIAM, 2000.

[22] R. Weber dos Santos, G. Plank, S. Bauer, and E. J. Vigmond, "Parallel multigrid preconditioner for the cardiac bidomain model," *IEEE Trans. Biomed. Eng.*, vol. 51, no. 11, pp. 1960–1968, Nov. 2004.

Martin J. Bishop received the M.Phys. degree in physics, in 2003, and the D.Phil. degree in computational biology, in 2008, both from the University of Oxford, Oxford, U.K.

He is currently a Sir Henry Wellcome Postdoctoral Fellow at the Computing Laboratory, University of Oxford. His current research interests include computational cardiac modelling and imaging.

Gernot Plank received the M.Sc. and Ph.D. degrees in electrical engineering from the Institute of Biomedical Engineering, Technical University of Graz, Austria, in 1996 and 2000, respectively.

He is currently an Associate Professor at the Institute of Biophysics, Medical University of Graz, and an Academic Fellow at the Oxford e-Research Centre, University of Oxford, Oxford, U.K. He was a Postdoctoral Fellow at the Technical University of Valencia, Valencia, Spain, from 2000 to 2002 and at the University of Calgary, AB, Canada, in 2003. He was also a Marie Curie Fellow at Johns Hopkins University, Baltimore, MD, from 2006 to 2008. His research interests include computational modelling of cardiac bioelectric activity, microscopic mapping of the cardiac electric field and defibrillation.